Available online at www.eccomasproceedia.org
Eccomas Proceedia COMPDYN (2023) 4017-4029

ECCOMAS
Proceedia

COMPDYN 2023
9th ECCOMAS Thematic Conference on
Computational Methods in Structural Dynamics and Earthquake Engineering
M. Papadrakakis, M. Fragiadakis (eds.)
Athens, Greece, 12-14 June 2023

NUMERICAL MODELLING OF POORLY DETAILED EXISTING RC BEAM-COLUMN JOINTS

Angiolilli M.[1], Gregori A.[2], Bizzarri L.[2], D'Agostino C.[2], Ciuffetelli E.[2], Peditto A.[2], Gualtieri P.[2]

[1] National Institute for Nuclear Physics (INFN) -Gran Sasso Laboratory (LNGS)
Via G. Acitelli, 67100 L'Aquila, Italy
e-mail: michele.angiolilli@lngs.infn.it

[2] Department of Civil, Construction and Environmental Engineering, University of L'Aquila
Monteluco di Roio 67100 L'Aquila, Italy
e-mail: amedeo.gregori@e-univaq.it, lorenzo.bizzarri@graduate.univaq.it,
caterina.dagostino@graduate.univaq.it, edoardo.ciuffetelli@univaq.it, alfredo.peditto@univaq.it,
pasqualino.gualtieri@univaq.it

Abstract.

The catastrophic collapse of existing reinforced concrete (RC) structures in areas with low to high seismic risk was often caused by the failure of beam-column joints, which are essential in transporting stresses and moments between those two main elements. Indeed, post-earthquake observations highlighted that most of the 1960s-70s Italian RC buildings, suffering significant damage levels during the last seismic sequences, were characterized by insufficient transverse reinforcing of the joints. In some cases, stirrups were even absent since were not prescribed by old design codes. Numerical three-dimensional finite element (FE) model for simulating crack propagation and fracture in concrete utilizing the smeared crack approach is used in this study to simulate an experimental test (part of a larger experimental campaign conducted by the University of L'Aquila) on exterior (i.e. façade) beam-column RC joint. In particular, according to the experimental assumptions, the FE model was developed to emphasize the vulnerability of the joints and, therefore, to achieve shear failure in the joint panel prior to yielding of both beam and column reinforcements. The model made it possible to examine specific assumptions on the mechanical performance of the RC joints. Numerical tests investigated the performance of the RC frame at different stage of the analysis (attainment of the first cracks as well as collapse condition) under both monotonic and cyclic tests aiming to investigate possible damage accumulation phenomena, that in turn, could affect the main mechanical properties of the sample. The results showed that the model well predicted the experimental outcomes, especially in terms of shear strength and crack propagation, and provided critical insight into the calibration of the numerical model under cyclic loads, mainly trough the investigation of a material property regulating the shear stiffness reduction after cracks.

Keywords: Cyclic, Reinforced Concrete, Earthquake Engineering, Damage accumulation, Energy dissipation, Nonlinear Analysis, Crack pattern, Shear retention factor

ISSN:2623-3347
Peer-review under responsibility of the organizing committee of COMPDYN 2023.
doi: 10.7712/120123.10699.20814

1 INTRODUCTION

Based on previous and recent earthquakes or studies, reinforced-concrete (RC) buildings demonstrated severe structural damage at both the local and global levels due to the potential brittle failure of vertical members, such as columns ((e.g., [1, 2]), whereas usability preventing and loss-providing damages are more frequent and primarily associated with the damage of nonstructural elements (e.g., [1, 3, 4, 5]). The behavior of beam-column intersections, or the so-called beam-column joint (BCJ) panel, on which this work is focused, is another significant factor that seems to have a significant impact on the seismic performance of existing frames, particularly in non-conforming buildings. Deficiencies mostly resulting from poor material qualities, insufficient or no transverse reinforcement at the BCJ panel, inappropriate anchor length/detail, among others, may cause catastrophic brittle failures linked to poor energy dissipation and sudden strength and stiffness degradation. Even under moderate seismic actions, such an adverse seismic behavior evidently affects the structural integrity of the entire system.

Reliable quantification of BCJ of non-conforming RC frames is critical for seismic vulnerability assessment. Therefore, the experimental performance of deficient joints has attracted considerable research interest especially for retrofitting purposes (e.g. [6, 7, 8, 9]). In the last two decades, several theoretical and empirical models have been proposed for evaluating the shear capacity of BCJ. A comprehensive overview of capacity models for shear strength of exterior RC joints is presented in [10], where uncertainties were also quantified by probabilistic procedures.

Those constitutive models are in general implemented in computer programs (e.g. [11, 12]) by which is still a challenge getting reliable simulations due to the general complexity of concrete behaviour associated with the crushing in compression, characterized by pronounced nonlinear behaviour also in the pre-peak stage, and quasi-brittle cracking in tension, with a decay of tensile capacity with the widening of the cracking process that, in turn, is followed by a decrease of crack shear stress transfer due to the deterioration of aggregate interlock. Furthermore, bar-slip phenomena and flexure-shear interaction in the members framing into the BCJ as well as various uncertainty sources (e.g. [9, 13]) strongly affect the simulations. The behavior of BCJ has been replicated numerically by using a variety of techniques, from straightforward to sophisticated finite or discrete element models [14, 15, 16]. Recent research has benefited from the advancement of computer-aided nonlinear analysis, which has been utilized to replicate the behavior of BCJ in multiaxial stress fields. The authors suggest to interested readers referring to [17] for a comprehensive overview of the various numerical approaches.

Furthermore, due to relatively scarce information based on experimental tests on gravity-load-designed frame systems and subassemblies, there is a general lack of appropriate modelling solutions for poorly designed beam-column joint system.

In this paper, an experimental test performed on a full-scale RC façade sub-assembly, tested under cyclic load up to its failure, is replicated through the use of a numerical three-dimensional model based on the concrete smeared crack (CSC) approach. A comparison between monotonic and cyclic numerical responses is provided. In particular, the effect of the shear stiffness reduction during cyclic loads (the so-called shear retention factor) is here investigated.

2 BRIEF DESCRIPTION OF THE RC FRAME EXPERIMENTALLY TESTED

A RC beam-column frame, representing an exterior subassembly isolated at the mid-points of members of a multi-storey building, was constructed and tested under the collaboration between the University of L'Aquila (Italy) and Tonelli Consulting company (Avezzano, Italy).

The beams with a cross-section of 300 x 500 mm^2 had an extension of 2,000 mm from the column face, whereas the columns had a cross-section of 300 x 500 mm^2 and a total height of 3,200 mm. A 300 x 500 mm ^{2} transversal beam extending 300 mm from the column face was also realized to better replicate the real geometry of existing RC frames.

Longitudinal reinforcement on both the two short sides of the column consisted of four steel rebars with 24 mm in diameter. Longitudinal reinforcement of the beams (both on top and bottom position) consisted of two bars of 24 mm in diameter plus three bars of 20 mm in diameter. The short transversal beam was reinforced by four bars with 16 mm in diameter, one in each of the corners. Transversal reinforcement for both columns and beams consisted of 10 mm in diameter and steel stirrups spaced 100 mm. It is noteworthy that stirrups were appositely not inserted in the joint panel, as justified above.

Specimens were tested imposing a precise sequence of increasing amplitude quasi-static cyclic displacements to a column-end (to simulate the seismic inter-floor drifts) in combination with null external forces applied to the column.

The load V was applied at the head column using an actuator with 500 kN capacity based on a displacement-controlled regime. Loading history details for all specimens were based on ACI 374.1 [18] and included several series of force sets, each one consisting of three fully reversed cycles (except the last three cycles, for which only one fully reversed cycles were applied for them). The drift ratio values were selected to evaluate the performance of the joints at different loading stages such as elastic response, before and beyond yielding, and failure. Here, the drift ratio was defined as the ratio between head column displacement and the length of the column by also considering the encumbrance of the support frames (i.e., total length of 3,340 mm). Note that [18] recommends that the end of the test should be at a drift ratio that equals or exceeds 3.5%. The diagonal deformation in the joint was measured by linear variable displacement transducers (LVDTs). Other LVDTs were also used to measure displacements of the head column and the two beam ends.

The experimental result showed an almost symmetrical cyclic behavior among the two load directions up to the attainment of the maximum strength V_{max} of 218 kN (for an imposed displacement d =177.4 mm). The initial hairline cracking in the BCJ panel started at 61.2 kN corresponding to about 0.4% of θ. For more details on the experimental campaign, the reader is referred to [19], where it was also provided a comparison in terms of V_{max} with the results of NTC2018 [20] and ACI-352R [21] prescriptions and other literature formulations (discussed in [10]). In particular, it was highlighted that the experimental test led to lower values with respect to the ones obtained by the various formulations (in some cases, the difference was pretty consistent).

3 DETAIL OF THE NUMERICAL MODEL

In this study, a numerical model was developed using the concrete smeared crack (CSC) model (implemented in the MIDAS FEA NX v1.1 software; release version: Nov 22 2022), which has been already successfully employed to simulate RC members under seismic loads (e.g. [22, 23, 24]).

With respect to the discrete models, in which the cracks are explicitly modelled merely through the separation of particles when tensile strength is reached, in the CSC approach, the extension of cracks is predicted by using the concept of fracture mechanics and studying the stress concentrations at the crack tip. Constitutive calculations are performed independently at each integration point of the finite element model. In the CSC model, the initiation of cracking process at any location happens when the concrete stresses reach one of the failure surfaces

either in the biaxial tension region or in a combined tension-compression region.

The CSC is used to simulate plain concrete and assumes that the monotonic load is applied to concrete under low confining pressure. The low confining pressure corresponds to the stress less than 1/5 to 1/4 of the maximum compressive strength of concrete. and it simulates the compression part of concrete using a typical isotropic elasto-plastic model, and the tensile part of concrete is simulated using a smeared crack model. The latter is a method of simulating the crack by adjusting the stress and stiffness at the integration point, without reconfiguring the mesh. In the CSC, the band-width obtained based on the size of the element is reflected in the crack behavior to avoid mesh dependencies ([11]). For a three-dimensional element, the cubic root of a volume is the crack width of the element. The compressive and tensile uniaxial behavior of the CSC model is shown in Fig. 1.

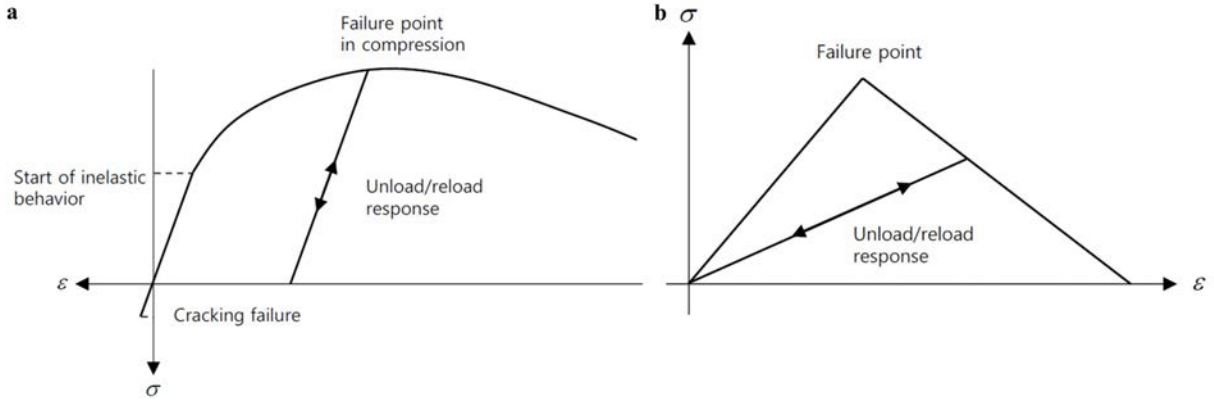

Figure 1: a) Uniaxial behavior of SCS; b) Tensile behavior of CSC.

Cracks occur when the stress is outside the crack detection surface, a type of yield function. If a crack occurs, the stress is returned using an implicit backward Euler method, and the direction of the maximum principal strain is the direction of the crack. This direction is stored to simulate the anisotropy by cracking in subsequent analyses. Since the orthogonal fixed crack model is used in this study, the subsequent crack shall be in a direction orthogonal to the existing crack direction and up to three in the case of the 3D model. If the elastic strain in the direction of the crack is tensile after the crack has occurred, it has behaved as damaged elastic and it is considered that the crack is closed when it is compressed.

In this study, the compression behavior of the plain concrete was modeled by the Thorenfeldt's law [26]. Note that in the preliminary calibration of the model [19], another constitutive model, namely JSCE-2017[27] was adopted (see an application in [28]). The compressive strength of concrete (f_c) was assumed according to the equivalent cylindrical compressive strength of tests performed on three samples, with an average value of 29.3 MPa.

The tensile behavior was instead modeled by the Hordijik's law [29] characterized by a linear hardening branch followed by a nonlinear softening branch. The area under the stress-strain curve should be equal to the fracture energy (G_f) divided by the equivalent length (according to the different size mesh adopted for the elements). According to CEB-FIP MC90, the concrete tensile strength f_t was defined as $0.3f_c^{(2/3)} = 2.85$MPa and G_f was assumed equal to 0.05 N/mm. The concrete elastic modulus was set as $E_{cm} = 22,000(0.1f_c)^{0.3} = 30,373$ MPa. Furthermore, concrete density $\gamma_c = 2.5e-3$ N/mm^3 and Poisson modulus ν_c =0.2.

In order to obtain the best balance between simulation accuracy and computational burden

as well as to thoroughly explore in particular the nonlinear behavior of the BCJ, following sensitivity analysis, it was decided to employ a different discretization of the RC sample.

In particular, eight-node solid brick elements with a maximum mesh size of 20 mm were specifically used to represent the joint up to an extension of 200 mm from its edges. Instead, the maximum mesh size at the beam and column ends, which extended respectively 1,200 mm and 770 mm, was 80 mm. The remaining center portion of the beam and column, with an extension respectively of 600 mm and 380 mm, had a maximum mesh size of 40 mm.

The steel rebars and ties are modelled as two-node one-dimensional embedded truss elements (do not require node sharing and are hence more convenient with respect to the conventional truss elements) which ignore flexural behavior. The tensile and compressive strengths were assumed according to B450C steel property defined in NTC2018 and characterized by yield strength $f_y = 450$ MPa, ultimate strength $f_u = 540$ MPa, elastic modulus $E_s = 210,000$ MPa, ultimate strain $\varepsilon_{s,u} = 0.75\%$, steel density $\gamma_s = 7.85e-5$ N/mm^3 and Poisson modulus ν_c =0.29. The embedded method with a perfect bond between reinforcement and surrounding concrete is adopted to simulate the reinforcement-concrete bonding interaction. It is notable that the effects usually associated with reinforcement-concrete interface, such as bond slip and dowel action cannot be directly modeled.

The stiffening effect provided by the steel plates at both the beam and column ends was simulated by introducing rigid links. In particular, a master node was applied in correspondence with the actuator's center of action at the top head column, whereas their respective slave nodes were located on the mesh nodes belonging to the top face of the column. Three further master nodes were applied in correspondence with the centre of the pinned support (at the base-column) and that of the roller supports at the two beam ends. Their respective slave nodes were applied to the mesh nodes belonging to the interested faces.

Regarding constraints: i) fixed translations along X and Z and fixed rotation along Y and Z were applied to the master nodes at the two beam ends; ii) fixed translations along X, Y, and Z and fixed rotations along Y and Z were applied to the master node at the base-column; iii) fixed translation along X was assumed to the master node at the head-column (note that this constraint was specifically introduced in this paper aiming to better represent the real cyclic behavior of the sample avoiding deflection along the gravitational direction after the joint failure).

Finally, note that the displacement d was applied in the master node at the top head column along Y direction, whereas gravitational loads were applied to all mesh nodes along negative X direction.

Fig. 2 shows the FE model and some details of both steel reinforcements and rigid-links simulating the steel plate stiffening.

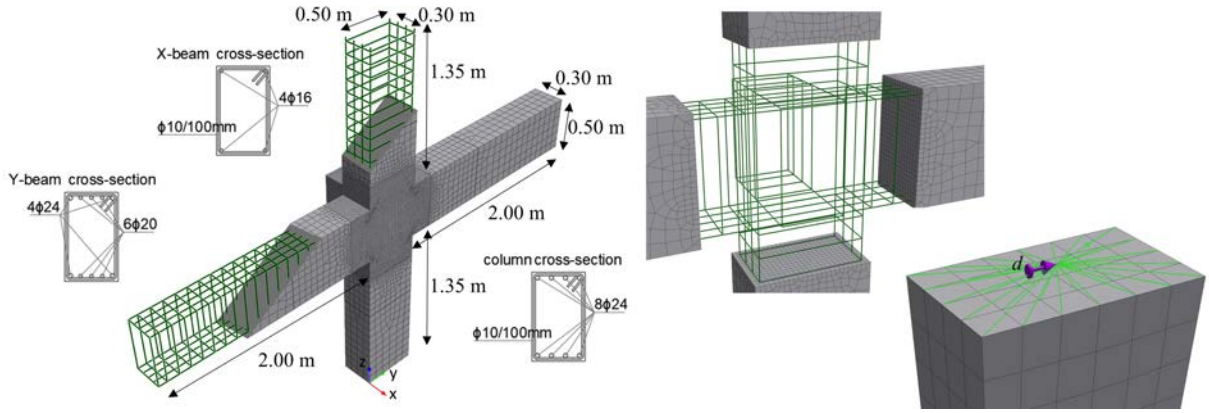

Figure 2: Numerical model with details of the geometry, the steel rebars and the rigid links at the column head

3.1 Effect of the cyclic shear reduction

A key feature of the cracking model is that, unlike crack initiation, which only considers Mode I fracture (tensile stress parallel to the crack plane), post-cracked behavior considers both Mode I and Mode II fracture (shear stress acting parallel to the plane of the crack and perpendicular to the crack front). The amount of crack opening, also function of the friction between the two surfaces of a crack and therefore very complex to predict in any damage model, determines the Mode II shear behavior. The dependence is that the shear modulus decreases as the crack expands. The post-cracked shear stiffness can therefore be calculated by the so-called shear retention model. Shear retention should theoretically decrease for large crack strains as less shear stress is capable of being transmitted across the crack. This phenomenon depends not only on the crack width but also on the transverse reinforcement ratio since the reinforcement provides additional strength.

Within smeared crack approach one can adopt rotating crack models (RCM) or fixed crack models (FCM). In contrast to RCM, which alters its orientation during loading in accordance with the principal stress directions, FCM used in the smeared crack technique maintains a stable crack orientation during the whole computational process. The RCM provides acceptable stress/strain rotations and a better prediction of model stiffness because of the shear retention function that provides coaxially between the principal stresses and strains. Acceptable FCM results can only be achieved when a near zero shear retention factor β is employed. In particular, β=0 refers to no aggregate interlock, whereas β=1 represents a full aggregate interlock. If the value of the shear retention factor is specified near to 1, there is a possibility of stress locking.

In [30] it was highlighted that the use of a variable shear retention factor (decreasing for increasing crack opening) allowed for the best fitting between numerical and experimental results (beams tested under 4-point bending). On the contrary, the use of a constant shear retention factor may result in a stiffer post-peak response and too little structural softening [31]. A study [32] recommended that an average value of 0.40 is to be taken into account in RC beams analysis, whereas other studies (e.g. [33]) suggest values between 0.2 and 0.3. However, the sensitivity of deformability and damage evolution as a function of constant β was explored in [30] finding out that the results are almost identical for values of β greater than 0.2 while lower values are ineffective. Finally, several studies (e.g. [34, 35]) showed that post-peak behavior could be satisfactorily simulated by assuming a very low β value (e.g., 0.001). Thereby, it can be concluded that the shear retention factor is an important parameter to be calibrated case by case depending on the loading and structure types based on which one should make a judgment in selecting this

parameter.

The model adopted in this study allows considering a shear retention factor. Hence, a parametric investigation was performed in terms of β, assuming for it constant values of 0.05, 0.2 or 0.4 as well as variable values through the relation developed in [36], for which shear stiffness decreases as a function of the normal total strain ε_{nn}, as follows: $\beta = 0.4(f_t/(E\varepsilon_{nn})$.

The following results are presented by using labels in which the first letter indicates the type of test (E=experimental; N=numerical), the second letter indicates the compressive constitutive law (J for JSCE-2017 or T for Thorenfeldt [26]). Then, it is specified the value assumed for the shear retention factor β.

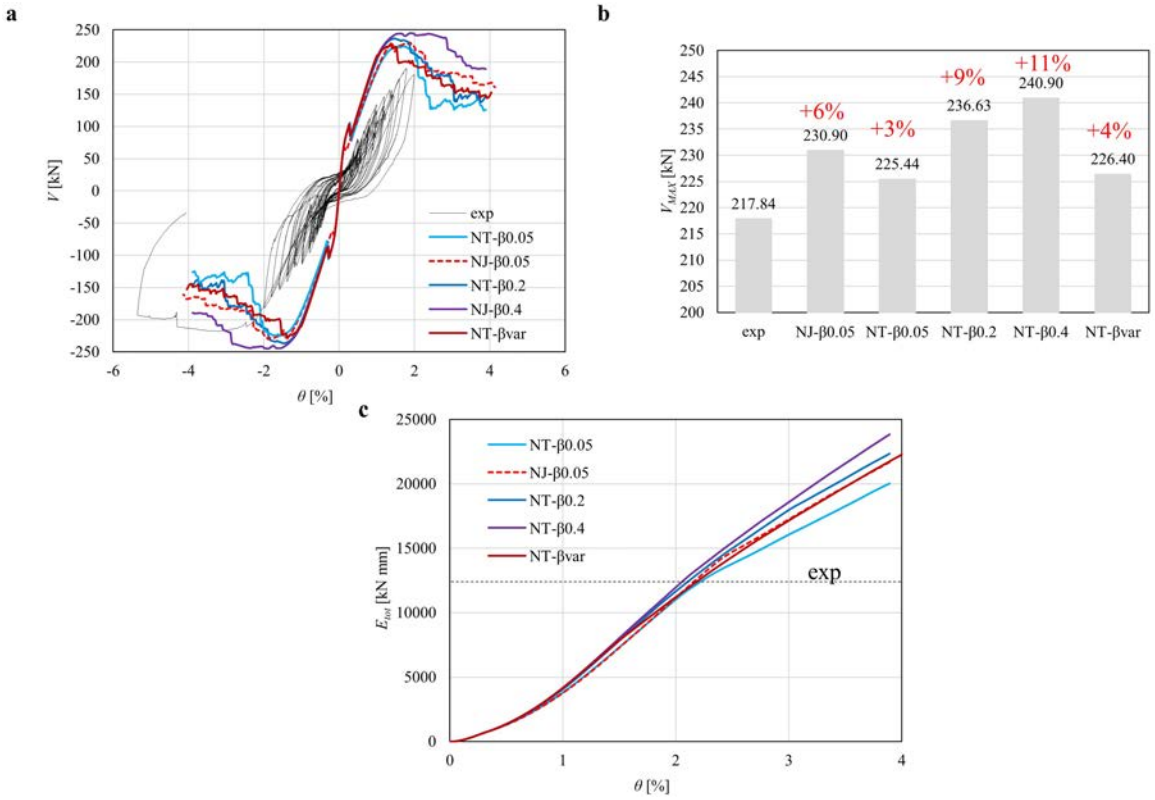

Figure 3: Comparison between cyclic experimental curve and monotonic numerical curves in terms of: a) $V - \theta$ curves; (b) shear strength values; c) Energy dissipation E_{tot}.

In particular, Fig. 3a shows the $V - \theta$ responses obtained numerically under monotonic load-condition as well as experimentally under cyclic test. It is important to highlight that also the response obtained in the initial calibration phase of the model [19] (i.e. the NJ-β0.05 case) is reported in Fig. 3a, noting that it was obtained by assuming JSCE-2017 constitutive law in compression, constant β value equal to 0.05, and through a different software version (v1.1, release: Oct. 23 2020). The different law in compression adopted in the present study was mainly due to the instability issue that occurred during numerical cyclic analysis (described later).

First of all, the main difference with respect to the experimental response regards the slope of the numerical curve, which is higher as compared to the experimental one. This could be depending on possible bar-slip phenomenon, which cannot be captured in the present model, as already commented in [19]. Among the numerical curves of Fig. 3a, one can see a slight

difference in terms of maximum strength and a more consistent difference in the post-peak behavior. In general, results suggest that the lower the constant value assumed for β, the lower the strength and load-bearing capacity according also to the literature studies described above. For all cases, a first stress drop is seen close to 100 kN and caused by the onset of cracks in the BCJ panel (as proven in [19]).

In Fig. 3b, a comparison in terms of shear strength V_{max} is shown. In particular, one can see that the best matching of the experimental value is obtained for the case with the lower β constant value (i.e., NT-β0.05) as well as with variable one (i.e., NT-βvar).

To further aid the evaluation of specimen performance under different β assumptions, the cumulative energy dissipation E_{tot}, was computed as the area enclosed by the global response, in terms of $V - d$ relationship. The comparison of the results was computed up to the same imposed displacement ($d = 130$mm). Specifically, also the value reported for the experimental case (about 12,000 kN mm) was computed for the envelope curve in the negative direction of the test (i.e., Y -, for which collapse occurred) and referred to a maximum value of $d = 130$mm. It is important to note that this specific imposed value allowed stable results avoiding numerical instability for all the investigated cases.

The simulation of cyclic tests was also carried out in quasi-static regime, in line with the experimental procedure (acceleration was almost negligible due to the comparatively slow applied load).In particular, only the initial sequence of the experimental test is presented in this study, as depicted in Fig. 4a where it can be observed the imposed d during the test (not symmetric between the positive and negative load direction). The experimental response of the first phase is shown in Fig. 4b, whereas the crack pattern is depicted in Fig. 4c, noting that only a few hair crack lines in the BCJ occurred in this preliminary phase. Then, in Fig. 4d is reported the measurement of the shear strain γ as the sum of the two strains ε (in absolute terms) measured along the two LVTDs mounted to the BCJ panel.

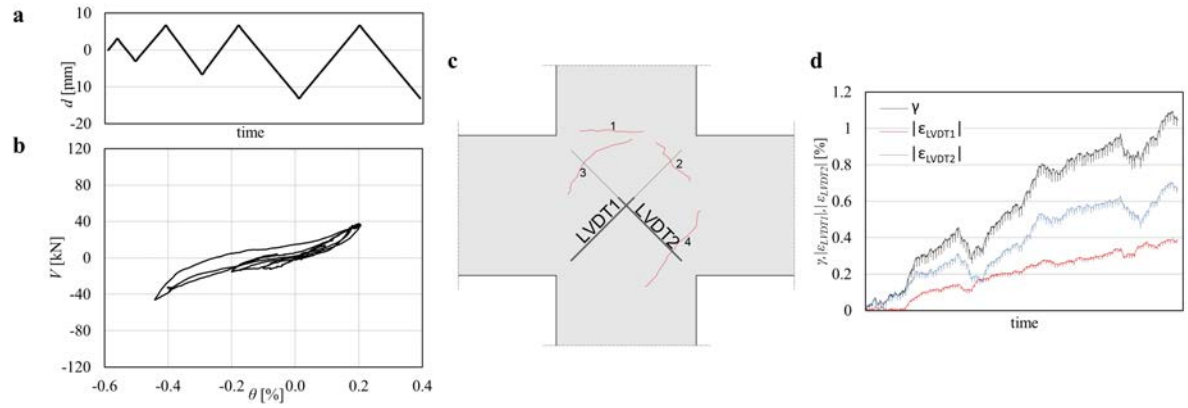

Figure 4: Details of the first cycles of the experimental test: a) imposed d during the test-time; b) $V - \theta$ curve; c) crack pattern at the BCJ; deformation of the BCJ

The numerical capacity curves are reported in Fig. 5a, where it can be observed that the lower the constant value of β, the higher the shear strength degradation achieved at the various cycles. Moreover, for all the investigated cases, one can observe a slight stiffness reduction at the various cycles.

In Fig. 5b, the numerical shear strain is reported as a function of the step analysis, showing a slightly lower value of γ achieved with respect to the experimental one (for which γ was about 1% at the end of the investigated phase, also taking into account possible erroneous movements

of the LVTDs). The case that better reproduced the experimental outcome is the NT-βvar one. In Fig. 5c it is shown the crack pattern of the only BCJ panel plotted up to 0.01 mm in crack width. In particular, one can see that for NT-β0.4 and NT-βvar cases, a more concentration of cracks occurs in the center of the BCJ, in line with the experimental evidence. This propensity can be observed also in Fig.6, where the crack pattern, Von Mises stress, and strain rebars are depicted. Indeed, from that figure it is pretty clear that the outcomes referred to low constant β values (i.e. NT-β0.05 and NT-β0.2) wrongly reproduced the experimental evidence since, unlike to that case, stress concentration and crack propagation interested also columns and beams of the RC frame as well as the rebar strain also exceeded the yield value and it was close to the ultimate condition.

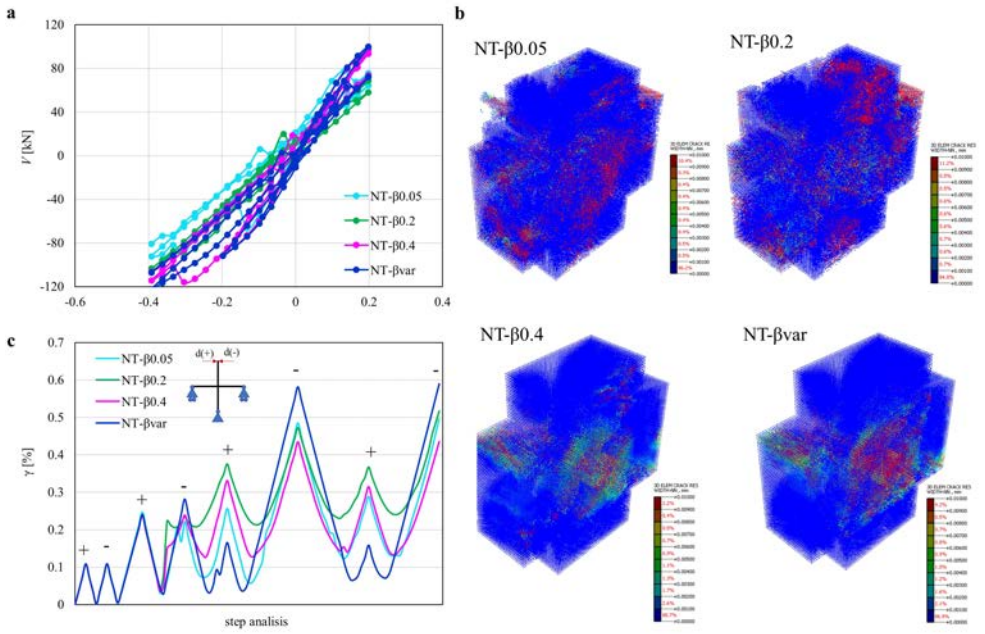

Figure 5: a) $V - \theta$ numerical curve; b) Crack pattern of the only BCJ panel; c) numerical shear strain

Therefore, despite a good match of the experimental outcome (especially in terms of shear strength) was obtained by assuming very low constant β values through numerical monotonic tests (see Fig. 3a), this assumption led to a completely wrong prediction of cyclic tests. On the contrary, by assuming variable β value (as a function of the normal total stain) a good prediction of both monotonic and cyclic tests was performed. Hence, future numerical studies performed by the Authors and focusing on the mechanical behavior of different typologies of RC beam-column joints under both unreinforced and reinforced conditions will consider this assumption for the shear retention factor.

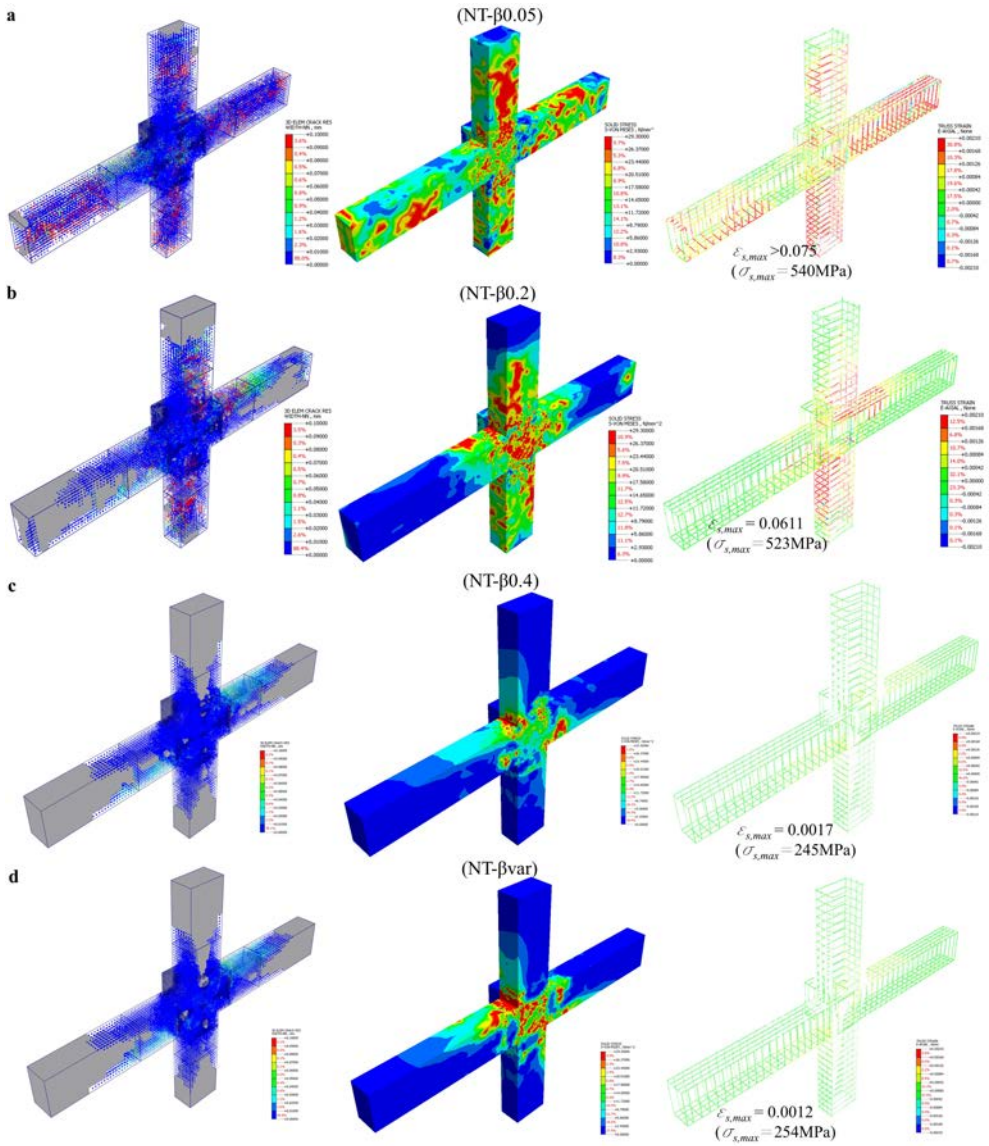

Figure 6: Crack pattern (right), Von Mises Stress (centre) and rebar strain (left) for the different investigated cases: NT-β0.05 (a), NT-β0.2 (b), NT-β0.4 (c), NT-βvar (d)

4 CONCLUSIONS

The numerical results of an RC beam-column joint connection are described in the current work. The joints' brittleness—typical of Italian reinforced concrete buildings from the 1960s to the 1970s—was emphasized to cause shear failure only in the junction panel before yielding both the beam and column reinforcements (differently from other tests described in the current literature). To simulate crack propagation and fracture in concrete as well as to comprehend some physical principles, a three-dimensional model utilizing the smeared crack technique was employed. A parametric numerical study was carried out to show how a particular parameter, the shear retention factor, affects both monotonic and cyclic tests. Indeed, it is worth noting that, despite the fact that very low constant values assumed for the shear retention factor, in monotonic tests, lead to the best matching of the experimental test, also in line with numerous literature findings, it is essential to assume variable values for it (as a function of the normal total strain of the elements or, in general, also in terms of crack wide) to properly simulate cyclic

tests. Indeed, apart from the increased numerical stability of the simulation, the best benefit in assuming variable values for it in cyclic tests is related to the very accurate simulation of stress concentration and fracture propagation in plane concrete as well as the good distribution of the stress to the rebars.

REFERENCES

[1] P. Ricci P., F. De Luca, G. M. Verderame, 6th April 2009 L'Aquila earthquake, Italy: Reinforced concrete building performance. *Bulletin of Earthquake Engineering* **9**(1), 285–305, 2011

[2] P. Ricci, M. Di Domenico, and G. M. Verderame, Empirical-based out-of-plane URM infill wall model accounting for the interaction with in-plane demand. *Earthquake Engineering & Structural Dynamics* **47**(3) 802–27, 2018

[3] F. Braga, , V. Manfredi, A. Masi, A. Salvatori, M. Vona, Performance of non-structural elements in RC buildings during the L'Aquila, 2009 earthquake. *Bulletin of Earthquake Engineering* **9**(1), 307-24, 2011

[4] R. Vicente, H. Rodrigues, H. Varum, A. Costa, J. A. R. Mendes da Silva, Performance of masonry enclosure walls: Lessons learned from recent earthquakes. *Earthquake Engineering and Engineering Vibration* **11**(1), 23–24, 2012

[5] M. Angiolilli, M. E. Minkada, M. Di Domenico, S. Cattari, A. Belleri, G. M. Verderame, Comparing the Observed and Numerically Simulated Seismic Damage: A Unified Procedure for Unreinforced Masonry and Reinforced Concrete Buildings. *Journal of Earthquake Engineering*, 1–37, 2022

[6] C. Del Vecchio, M. Di Ludovico, A. Balsamo, A. Prota, G. Manfredi, M. Dolce, Experimental investigation of exterior RC beam-column joints retrofitted with FRP systems. *Journal of Composites for Construction* **18**(4), 04014002, 2014

[7] C. Del Vecchio, M. Di Ludovico, A. Balsamo, A. Prota, Seismic retrofit of real beam-column joints using fiber-reinforced cement composites. *Journal of Structural Engineering* **144**(5) 04018026, 2018

[8] O. Yurdakul, O. Avsar, Strengthening of substandard reinforced concrete beam-column joints by external post-tension rods. *Engineering Structures* **107**, 9–22, 2016

[9] O. Yurdakul, C. Del Vecchio, M. Di Ludovico, O. Avsar, Numerical simulation of substandard beamcolumn joints with different failure mechanisms. *Struct Concrete* **21**(6), 2515–2532, 2020

[10] C. Lima, E. Martinelli, C. Faella, Capacity models for shear strength of exterior joints in RC frames: state-of-the-art and synoptic examination. *Bulletin of Earthquake Engineering* **10**, 967–983, 2012

[11] Z. Bažant, B. H. Oh, Crack band theory for fracture of concrete. *Matériaux et construction* **16**, 155–177, 1983

[12] A. Hillerborg, M. Modéer, P. E. Petersson, Analysis of crack formation and crack growth in concrete by means of fracture mechanics and finite elements. *Cement and concrete research* **6**(6), 773–781, 1976

[13] A. Rimkus, V. Cervenka, V. Gribniak, J. Cervenka, Uncertainty of the smeared crack model applied to RC beams. *Engineering Fracture Mechanics* **233**,107088, 2020

[14] S. J. Pantazopoulou, J. F. Bonacci, On earthquake-resistant reinforced concrete frame connections. *Canadian Journal of Civil Engineering*, **21**(2), 307–328, 1994.

[15] M. Youssef, A. Ghobarah, Modelling of RC beam-column joints and structural walls. *Journal of earthquake engineering*, **5**(01), 93–111, 2001

[16] G. Calvi, G. Pampanin, Experimental test on a three storey RC frame designed for gravity only. *12th European Conference on Earthquake Engineering* London, paper n. 727, 2002

[17] A. E. Behbahani, J. A. Barros, A. Ventura-Gouveia, Plastic-damage smeared crack model to simulate the behaviour of structures made by cement based materials. *International Journal of Solids and Structures* **73** 20–40, 2015

[18] ACI 374.1, Acceptance Criteria for Moment Frames Based on Structural Testing and Comm. *American Concrete Institute*, Farmington Hills, 2005.

[19] M. Angiolilli, A. Gregori, R. Tonelli, C. Tonelli, E. Ciuffetelli, A. Peditto, Structural performance of unreinforced full-scale façade concrete beam-column joint under cyclic load. *Procedia Structural Integrity* **44**, 870–877, 2023

[20] NTC, Norme tecniche per le costruzioni in zone sismiche, in Italian, Ministerial Decree DM; 2018.

[21] ACI 352R-02, Recommendations for Design of Beam-Column Connections in Monolithic Reinforced Concrete Structures, ACI-ASCE Committee, 2002

[22] M. Asgarpoor, A. Gharavi, S. Epackachi, A simplified model for concrete at low confining pressures. *Structures* **29**, 1322–1351, 2021

[23] F. Di Carlo, A. Meda, Z. Rinaldi, Numerical cyclic behaviour of un-corroded and corroded RC columns reinforced with HPFRC jacket. *Composite Structures* **163**, 432–443, 2017

[24] A. Earij, G. Alfano, K. Cashell, X. Zhou, Nonlinear three–dimensional finite–element modelling of reinforced–concrete beams: Computational challenges and experimental validation. *Engineering Failure Analysis* **82** 92–115, 2017

[25] H. D. Hibbitt, A simplified model for concrete at low confining pressures. *Nuclear engineering and design* **104**, 313–320, 1987

[26] E. Thorenfeldt, A. Tomaszewicz, J. J. Jensen, Mechanical properties of highstrength concrete and applications in design. *In Proc. Symp. Utilization of HighStrength Concrete, Stavanger, Norway*, 1987

[27] JSCE, Guideline on Design and Application Methods of Silicate-based Surface Penetrants used for Concrete Structures. *Japan Society of Civil Engineers*, Concrete Library 137, 2017

[28] Fu, L., Nakamura H., Yamamoto Y., M. Taito, Effect of various structural factors on shear strength degradation after yielding of RC members under cyclic loads. *Journal of Advanced Concrete Technology* **18**, 211–226, 2020

[29] D. A. Hordijk, Local approach to fatigue of concrete. *Delft University of Technology, The Netherlands*, 1991

[30] R. Scotta, R. Vitaliani, A. Saetta, E. Oñate, A. Hanganu, A scalar damage model with a shear retention factor for the analysis of reinforced concrete structures: theory and validation. *Computers & structures* **79**(7), 737–755, 2001

[31] J. G. Rots, R. De Borst, Analysis of mixed-mode fracture in concrete. *Journal of engineering mechanics* **113**(11), 1739–1758, 1987

[32] S. Khalfallah, A. Charif, N. Mohammed, Nonlinear analysis of reinforced concrete structures using a new constitutive model. *Revue Européenne des Eléments* **13**(8), 841–856, 2004

[33] L. Dahmani, A. Khennane, S. Kaci, Crack identification in reinforced concrete beams using ANSYS software. *Strength Mater* **42**(2), 232–240, 2010

[34] N. Mitra, L. N. Lowes, Factors influencing analytical continuum simulation of three-point bend test of a concrete notched beam. *14th World Conference on Earthquake Engineering*, Beijing, China, October, 2008.

[35] J. G. Rots, P. Nauta, G. M. A. Kuster,J. Blaauwendraad, Smeared crack approach and fracture localization in concrete. *HERON* **30**(1), 1985

[36] R. S. H. Al-Mahaidi, Nonlinear Finite Element analysis of reinforced concrete deep members. *Cornell University*, 1978

[37] T. Paulay, M.J.N. Priestley, Seismic design of reinforced concrete and masonry building. *John Wiley & Sons, inc.*, New York, 1992

[38] M. J. N. Priestley, Myths and fallacies in earthquake engineering, revisited. *The Mallet Milne Lecture. IUSS Press: 58 Pavia, Italy*, 2003